The AAPS Journal (2020) 22: 8
DOI: 10.1208/s12248-019-0393-z

Research Article

Theme: Natural Products Drug Discovery in Cancer Prevention
Guest Editors: Ah-Ng Tony Kong and Chi Chen

Epigenome and transcriptome study of moringa isothiocyanate in mouse kidney mesangial cells induced by high glucose, a potential model for diabetic-induced nephropathy

Shanyi Li,[1] Wenji Li,[1,2,3] Renyi Wu,[1] Ran Yin,[1] Davit Sargsyan,[1,4] Ilya Raskin,[5] and Ah-Ng Kong[1,6]

Received 22 August 2019; accepted 9 November 2019; published online 5 December 2019

Abstract. Moringa isothiocyanate (MIC-1) is a bioactive constituent found abundantly in *Moringa oleifera* which possesses antioxidant and anti-inflammation properties. However, epigenome and transcriptome effects of MIC-1 in kidney mesangial cells challenged with high glucose (HG), a pre-condition for diabetic nephropathy (DN) remain unknown. Herein, we examined the transcriptome gene expression and epigenome DNA methylation in mouse kidney mesangial cells (MES13) using next-generation sequencing (NGS) technology. After HG treatment, epigenome and transcriptome were significantly altered. More importantly, MIC-1 exposure reversed some of the changes caused by HG. Integrative analysis of RNA-Seq data identified 20 canonical pathways showing inverse correlations between HG and MIC-1. These pathways included GNRH signaling, P2Y purigenic receptor signaling pathway, calcium signaling, LPS/IL-1-mediated inhibition of RXR function, and oxidative ethanol degradation III. In terms of alteration of DNA methylation patterns, 173 differentially methylation regions (DMRs) between the HG group and low glucose (LG) group and 149 DMRs between the MIC-1 group and the HG group were found. Several HG related DMRs could be reversed by MIC-1 treatment. Integrative analysis of RNA-Seq and Methyl-Seq data yielded a subset of genes associated with HG and MIC-1, and the gene expression changes may be driven by promoter CpG status. These genes include Col4a2, Tceal3, Ret, and Agt. In summary, our study provides novel insights related to transcriptomic and epigenomic/CpG methylomic alterations in MES13 upon challenged by HG but importantly, MIC-1 treatment reverses some of the transcriptome and epigenome/CpG methylome. These results may provide potential molecular targets and therapeutic strategies for DN.

KEY WORDS: diabetic nephropathy; moringa isothiocyanate; epigenome; transcriptome.

Guest Editors: Ah-Ng Tony Kong and Chi Chen

Electronic supplementary material The online version of this article (https://doi.org/10.1208/s12248-019-0393-z) contains supplementary material, which is available to authorized users.

[1] Department of Pharmaceutics, Ernest Mario School of Pharmacy, Rutgers, The State University of New Jersey, 160 Frelinghuysen Road, Piscataway, New Jersey 08854, USA.
[2] Institute of Translational Medicine, Medical College, Yangzhou University, Yangzhou, 225001, People's Republic of China.
[3] Jiangsu Key Laboratory of Integrated Traditional Chinese and Western Medicine for Prevention and Treatment of Senile Diseases, Yangzhou University, Yangzhou, 225001, People's Republic of China.
[4] Graduate Program in Pharmaceutical Science, Ernest Mario School of Pharmacy Rutgers, The State University of New Jersey, Piscataway, New Jersey 08854, USA.
[5] Department of Plant Biology & Pathology, Rutgers, The State University of New Jersey, New Brunswick, New Jersey 08901, USA.
[6] To whom correspondence should be addressed. (e–mail: KongT@pharmacy.rutgers.edu)

Abbreviations: *DEGs*, Differential expressed genes; *DMRs*, Differentially methylation regions; *DN*, Diabetic nephropathy; *DSS*, Dextran sulfate sodium; *ESRD*, End-stage renal disease; *HG*, High glucose; *IPA*, Ingenuity Pathway Analysis; *ROS*, Reactive oxygen species; *TSS*, Transcription start site; *LG*, Low glucose; *MIC-1*, Moringa isothiocyanate; *MES13*, Mesangial cells; *NGS*, Next-generation sequencing; *Nrf2*, Nuclear factor (erythroid-derived 2)-like 2.

INTRODUCTION

Diabetic nephropathy (DN) is one of the leading causes of end-stage renal disease (ESRD) accounting for about half of all ESRD cases with ESRD 5-year survival being less than 40% in the USA (1–3). Approximately 40% of diabetics develop DN with an estimated 6.9 million Americans having the disease from 2005 to 2008 (3). Currently, treatment modalities for DN are very limited. Many studies have shown that hyperglycemia can play a dominant role in the occurrence and development of DN (4,5). In addition, researchers have shown an increased interest in inflammation and oxidative stress potentially driving the development of DN (6–8). Most recently, epigenetic regulation including methylation, noncoding RNAs, and histone modifications have also been implicated in the occurrence and development of DN (9,10).

Some epigenetic small molecular and natural bioactive constituents may alter epigenetics, which can be used as promising therapeutic targets (11). Previously, we have shown that several dietary phytochemicals offer promising benefits in modulating epigenetics in the prevention/treatment of human diseases (12,13). *Moringa oleifera* has been used as vegetable and traditional herbal medicine and may possess many health benefits. Moringa isothiocyanate (MIC-1) is predominantly found in *Moringa oleifera*, which is used in traditional herbal medicine as anti-cancer, anti-inflammatory, and antidiabetic (anti-hyperglycemic) botanical (14,15). A study showed that an aqueous extract of *M. oleifera* leaves reduced fasting plasma glucose, increased reduced glutathione, and decreased malondialdehyde compared with control (16). Since, MIC-1, like most of the isothiocyanates (ITCs), would be a soft electrophile and our previous study shows that MIC-1 activates nuclear factor (erythroid-derived 2)-like 2 (Nrf2) antioxidant response element signaling, increases expression of Nrf2 target genes, and suppresses LPS-induced expression of inflammation in RAW 264.7 cell (17). More importantly, the results showed that TGFβ1 signaling is activated by high glucose (HG) and MIC-1 can inhibit HG-stimulated TGFβ1 activation in human renal proximal tubule HK-2 cells (17). In addition, MIC-1 treatment in mouse epidermal JB6 P+ cells showed that MIC-1 can protect against 12-O-tetradecanoylphorbol-13-acetate-induced neoplastic transformation, cancer, and inflammatory-mediated pathways (18). However, there is little information on transcriptomic and CpG methylome effects associated with MIC-1 in the prevention/treatment of a cell-cultured model of DN induced by HG.

Mesangial cells (MES13) are well-characterized SV40-transformed mouse kidney mesangial cells, and kidney mesangial cell is one of the main types of cells that are used to study DN development (19). It is a widely accepted *in vitro* model for DN (20,21). It has been reported that lysophosphatidic acid increases MES13 cell proliferation via Rac1/MAPK/KLF5 signaling pathway which could be associated with glomerular hyperplasia during DN (19). *In vitro* studies have shown that sustained Wnt/β-Catenin signaling reduced c-Jun-dependent TGFβ1-mediated fibronectin accumulation in HG stress-induced MES13 (22). MES13 activated metabolic pathways associated with oxidative stress in a high extracellular glucose environment (23). Recently, with next-generation sequencing (NGS), one can get large and rich data sets that allow assessment of gene expression patterns in RNA-Seq and epigenetic CpG methylation profiles via bisulfite modification (24,25). A better understanding of how HG drives the development of DN will help to explore the potential prevention/treatment methods of DN in human patients. Moreover, the antioxidant and anti-inflammatory capacity of MIC-1 and its gene expression profiling have not been investigated in the MES13 cell model in HG condition. In this study, we investigated the transcriptome and DNA methylome profiles and the potential preventive effects of MIC-1 in HG-induced MES13 cell model which simulates DN in human (20,21,26).

MATERIAL AND METHODS

Materials

Dulbecco's modified Eagle's medium (DMEM), penicillin-streptomycin, fetal bovine serum (FBS), and trypsin-EDTA were acquired from Gibco (Grand Island, NY, USA). MIC-1 (98% purity) was provided by Ilya Raskin (Rutgers University). CellTiter® 96 Aqueous One Solution Cell Proliferation Assay kit (MTS) was obtained from Promega (Madison, WI, USA). AllPrep DNA/RNA Mini kit was obtained from Qiagen (Valencia, CA). Illumina TruSeq RNA preparation kit was obtained from Illumina (San Diego, CA, USA). Agilent Mouse SureSelect Methyl-Seq Target Enrichment System was obtained from Agilent (Santa Clara, CA).

Cell Culture and Treatment

SV40-transformed mouse kidney MES13 were purchased from the American Type Culture Collection (Manassas, VA, USA) and cultured in DMEM with 14 mM HEPES and 5% FBS. Mes13 (1×10^5 cells) were seeded in a 10-cm dish and incubated overnight to allow their adherence. After incubation, the cells were treated with 5.5 mM D-glucose plus 24.5 mM D-mannitol as the low glucose group (LG), 30 mM D-glucose as the HG group, or HG with 1.5 μM MIC-1 as the MIC-1 group. 0.1% DMSO was added to each group as the vehicle control. The medium was changed every other day.

Cell Viability Assay

The cell viability was measured by MTS assay. Briefly, cells (1×10^3 cells/well) were seeded in a 96-well plate. After overnight incubation, the cells were treated with 0.1% DMSO or MIC-1 at various concentrations in DMEM with 1% FBS. The cell culture medium was changed every other day. To determine cell viability, MTS was performed after 1, 3, or 5 days of treatment according to the manufacturer's instructions.

Intracellular Reactive Oxygen Species Detection by Flow Cytometry and Confocal Microscopy

The intracellular reactive oxygen species (ROS) detection was modified from our previously reported method (17,27). Briefly CM-H2DCFDA (Invitrogen) was applied as

the ROS probe. MES13 were treated with 0.1% DMSO in LG, 0.1% DMSO in HG, or MIC-1 (0.5 μM, 1 μM and 1.5 μM in 0.1% DMSO in HG) for 48 h. The cells were grown to 90% confluence, washed with PBS, and then harvested using trypsinization, according to the manufacturer's protocol. The cells were then washed four times and incubated with 10 μM CM-H2DCFDA for 45 min at 37°C in a relatively high humidity (95%) atmosphere containing a controlled level of CO2 (5%) in the dark. Finally, cell-associated mean fluorescent intensity was measured by flow cytometry (Beckman Coulter, Brea, CA). ROS was also observed by a laser confocal microscope. The cells were incubated for 30 min in the dark at 37°C. Fluorescence images were obtained with a confocal microscope (FV-300, Olympus America, Melville, NY, USA); the sample was excited at a wavelength of 488 nm and capturing the fluorescence emission at 525 nm.

RNA-Seq Analysis

MES13 were stimulated with or without MIC-1 for 5 days. Then, total RNA was extracted from LG, HG, and MIC-1-treated MES13 using the AllPrep RNA Mini kit. Pooled RNA from 3 independent samples was used for library preparation. The mRNA sequencing libraries were constructed by the IlluminaTruSeq RNA preparation kit. The qualities of the prepped library cDNA were determined using the 2100 Bioanalyzer. The samples were sequenced on the Illumina NextSeq 500 system with a 75-bp paired-end reads with a minimum depth of 25–30 million reads per sample. Data quality was checked using the FastQC 0.11.2 software. The reads were compared with mouse genome (mm10) provided by the UCSC database and treated by HISAT2. Differential gene expression analysis was performed by the DESeq of R package as previously reported (28,29). For statistical analysis, two comparisons (HG *vs.* LG, MIC-1 *vs.* HG) were analyzed by p value and false discovery rate (q-value) as described by Storey *et al.* (30).

DNA Methylation Analysis

This assay was carried out in accordance with previous reports (28,29). Total DNA was extracted from LG, HG, and MIC-1-treated MES13 on day 5 using AllPrep DNA Mini kit. Pooled DNA from 3 independent samples was used for library preparation. The genomic DNA libraries were constructed by the SureSelect Methyl-Seq Target Enrichment System and sequenced with an IlluminaNextSeq 500 instrument with 76-bp single-end reads, generating 34–47 million reads per sample. Briefly, 1 μg of genomic DNA from 3 plates of cells' pooled DNA in each group was fragmented to the size of 100~175 bp and hybridized following the manufacturer's instructions. The Methyl-Seq Target Enrichment System targets 109 MB of mouse genomes or 3.3 million CpG sites. Bismark (version 0.15.0) alignment algorithm was used to compare DNA sequences with the bisulfite converted reference mouse genome (mm10). After comparison, the methylation counts were extracted using DMRfinder (version 0.1), and the CpG sites were clustered into the differentially methylation regions (DMRs) (31). Each DMR contained at least three CpG sites. Genome annotation analysis was conducted in R with ChIPseeker (1.10.3). Methylation ratio differences greater than 10% and with p value less than 0.05 were considered significant.

Pathway Analysis by Ingenuity Pathway Analysis

The gene expression levels with |log2 fold changes| ≥ 0.3 were investigated by the Ingenuity Pathway Analysis software (IPA 4.0, Ingenuity Systems). The canonical pathways associated with HG-induced subtypes and MIC-1 interventions were identified.

Correlation Between DNA Methylation and RNA Gene Expression

The RNA gene expression levels from RNA-Seq analysis were selected with a cutoff of |log2 (fold change)| ≥ 1. Then, the sorted genes from the RNA-Seq were further sorted by a cutoff of methylation ratio difference (%) ≥ 10 for DNA methylation changes. The genes of promoter DNA hypermethylation/RNA downregulation or promoter DNA hypomethylation/RNA up-regulation were selected as genes of interest for further analysis. The results were plotted in R.

Statistical Analysis

All values are expressed as the means ± standard deviation. Statistical analysis between groups was performed by Student's t test. $^{*}p < 0.05$ and $^{**}p < 0.01$ were considered to be statistically significant.

RESULTS

Cytotoxicity of MIC-1

As shown in Fig. 1, the MTS assay of cell activity after MIC-1 treatment was time-dependent and dose-dependent. After 1-, 3-, and 5-day treatment, the cell viability of MES13 was higher than 70% at a dose of 2 μM. Therefore, MES13 treated with MIC-1 (1.5 μM) for 5 days were used in our RNA-Seq and Methyl-Seq studies.

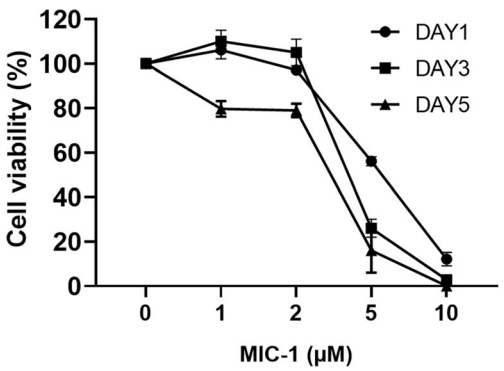

Fig. 1. Effect of MIC-1 on the viability of MES13. MES13 were treated with MIC-1 at different concentrations for 1, 3, and 5 days. The cell viability was measured by MTS assay. Data are expressed as mean ± standard deviation

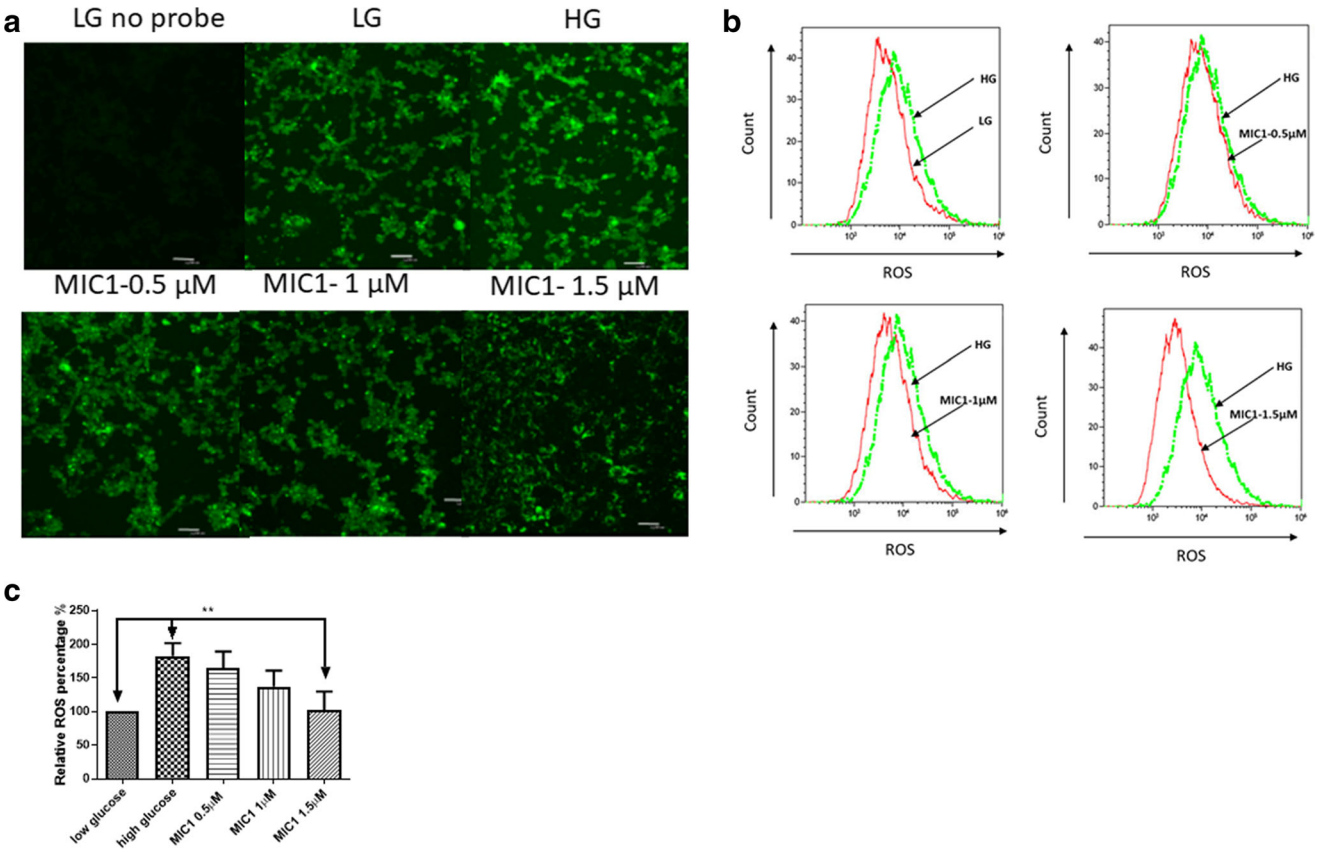

Fig. 2. Effects of MIC-1 on the production of intracellular ROS induced by 2-day treatment of MES13 with HG using confocal microscope (**a**) and flow cytometry (**b**). Two-day treatment with HG could increase intracellular ROS compared with the LG group. Treatment with 1.5 μM MIC-1 protected MES13 against ROS induced with HG. Relative ROS fold change normalized by the LG group are expressed as means ± standard deviation for three independent replicates, and significant ($p < 0.01$, **) differences compared with HG are indicated (**c**)

MIC-1 Reverses Intracellular ROS Enhanced by HG

The probe CM-H2DCFDA can penetrate membranes of mouse kidney MES13 and be converted into DCFH (2′,7′-dichlorodi-hydrofluorescein diacetate), a ROS reactive charged intermediate in living cells. The activated form can further react with ROS and be transformed into DCF (2′-7′-dichlorofluorescein), a fluorescent oxidized form, which can be detected by confocal microscopy and flow cytometry. In Fig. 2a, by confocal microscopy, there is no fluorescent signal in LG without probe and low signal in the LG group with probe, indicating that in normal mouse kidney mesangial cells, ROS production is relatively low. When cells were treated with HG, the signal was much higher indicating increased ROS production by HG. The increased signal could be reversed by MIC-1 treatment especially at 1.5 μM concentration (Fig. 2a). These findings are confirmed by flow cytometric assay, in which it indicates that a 2-day treatment of HG can generate a 2-fold increase of intracellular ROS as compared with LG group, while co-treatment of 1.5 μM MIC-1 in 0.1% DMSO in HG protected MES13 against ROS induced by HG ($p < 0.05$) (Fig. 2b, c).

Characteristics of Transcriptomic Changes Induced by HG and MIC-1 Exposure

To measure the gene expression profiles associated with HG and MIC-1 treatment, we performed RNA-Seq of MES13 stimulated by LG (control), HG, or HG with MIC-1. As shown in Fig. 3a, the observed variables of all the three groups are clearly separated from each other by principal component analysis (PCA). To further evaluate the gene expression profile of MES13, we also used Euclidean distance clustering to investigate the effect caused by HG with MIC-1 treatment. The result showed that the MIC-1 group clustered separately from LG and HG treatments (Fig. 3b). Next, we compared the global gene expression in all the three groups using a cutoff threshold *q-v*alue 0.25 and |log2 fold change| ≥ 0.3. As shown in the MA plots in Fig. 3c, compared with the LG group, there were 112 upregulated genes, 99 downregulated genes, and 12,991 unchanged genes in the HG group. Compared with the HG group, there were 415 upregulated genes, 296 downregulated genes, and 12,572 unchanged genes in the MIC-1 group (Fig. 3d). Top 10 genes with the highest and lowest log2 fold change were cataloged in Table I (HG *vs.* LG) and these genes included Fgl2 (involved in immune-regulation) and Smyd1 (a histone methyltransferase) that are potentially involved in DN induced by HG. Table II (MIC-1 *vs.* HG) included genes such as Gsta1 (antioxidant response) and Fgl2 that are potentially involved in MIC-1 response.

Effects of HG on Gene Expression and the Regulation by MIC-1

To study the possible biological function of MIC-1, we examined the impact or reverse effects of MIC-1 on HG-induced MES13 using a cutoff threshold *p* value 0.05 and |log2 fold

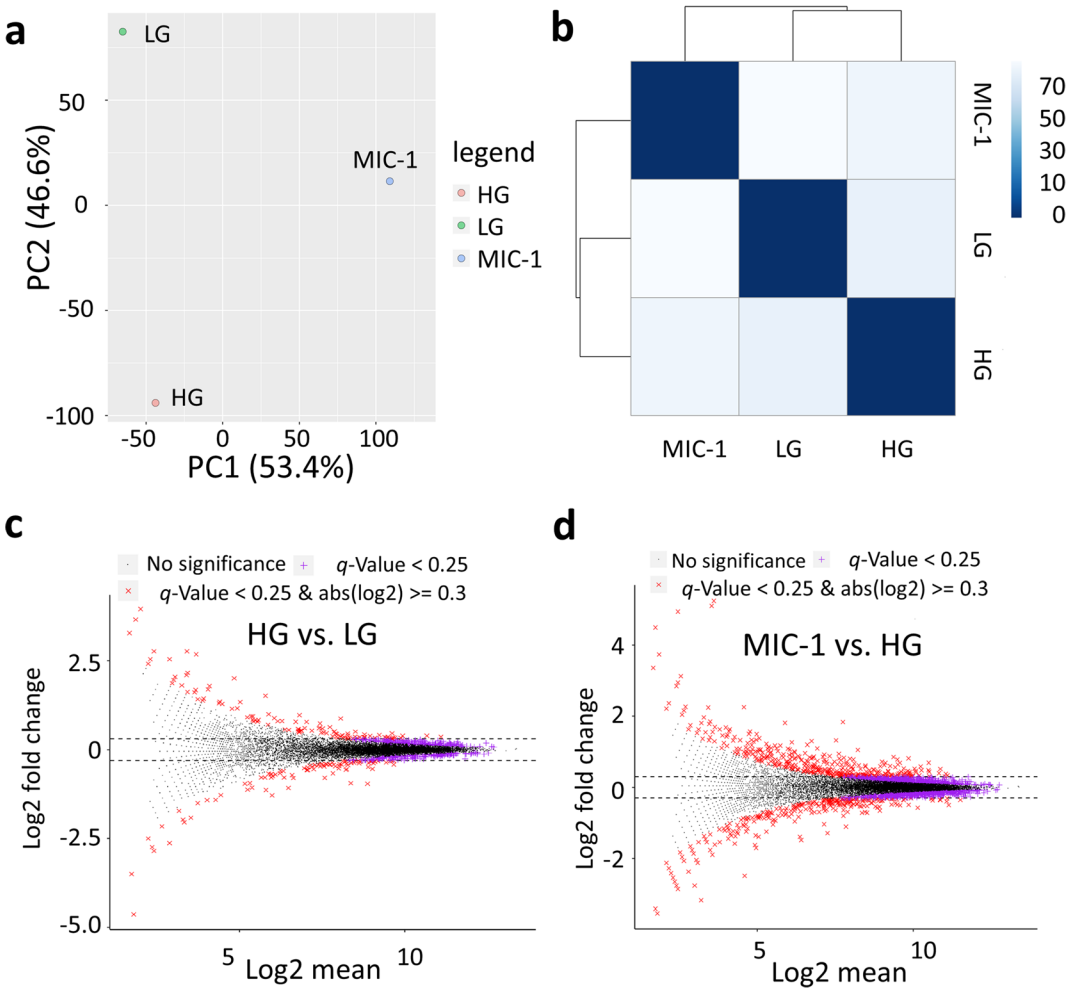

Fig. 3. Global transcriptomic change induced by HG and MIC-1 in MES13. **a** PCA for RNA-Seq analysis in the 3 groups. **b** Euclidean distance clustering between pairs of the 3 groups. MA plots for differential expression analysis of HG *vs.* LG (**c**) and MIC-1 *vs.* HG (**d**)

change| ≥ 0.5. As shown in Fig. 4a, 13 genes that were significantly downregulated by HG (13/259) were upregulated after MIC-1 treatment (13/98). In addition, 20 genes that were upregulated by HG (20/210) were downregulated after MIC-1 treatment (20/166) (Fig. 4b). These 33 reverse genes following MIC-1 treatment were shown in Fig. 4c. These genes including Fgl2, Kap (a kidney-specific androgen-regulated gene), and Tubb4a (a key component of the cytoskeleton) are potentially

Table I. HG *vs.* LG: Top 10 Upregulated Genes and Top 10 Downregulated Genes

Gene names	log2 (fold change)	*p* value	*q*-value (Storey *et al.* (2003))	Gene names	log2 (fold change)	*p* value	*q*-value (Storey *et al.* (2003))
Fam159b	3.96	1.04E-04	1.33E-02	Zic2	− 4.63	3.87E-04	3.25E-02
Hsd3b2	3.66	6.60E-04	4.84E-02	Grin1	− 3.50	1.78E-03	9.15E-02
C4b	3.28	4.24E-03	1.52E-01	Il23r	− 2.85	1.32E-03	7.62E-02
Acsm2	2.77	1.03E-05	2.38E-03	Smyd1	− 2.74	2.41E-03	1.11E-01
Ces2f	2.77	1.81E-03	9.18E-02	Ankrd61	− 2.63	4.84E-04	3.88E-02
5330417C22Rik	2.68	2.47E-06	8.90E-04	Olfr99	− 2.50	7.95E-03	2.05E-01
Akap5	2.54	7.25E-04	5.19E-02	Myo7b	− 2.50	7.95E-03	2.05E-01
Sox21	2.54	5.78E-03	1.79E-01	Mamdc2	− 2.50	7.95E-03	2.05E-01
Gm19589	2.42	1.03E-02	2.31E-01	C1qtnf3	− 2.16	8.25E-03	2.08E-01
Fgl2	2.42	1.03E-02	2.31E-01	Bmp8b	− 2.16	8.25E-03	2.08E-01

Table II. MIC-1 *vs.* HG: Top 10 Upregulated Genes and Top 10 Downregulated Genes

Gene names	log2 (fold change)	*p* value	*q*-value (Storey *et al.* (2003))	Gene names	log2 (fold change)	*p* value	*q*-value (Storey *et al.* (2003))
Gsta1	5.25	2.74E-19	2.26E-16	Ano9	− 3.54	1.23E-03	2.62E-02
Gm3776	5.11	1.61E-17	8.59E-15	Fgl2	− 3.42	2.29E-03	4.07E-02
Gsta2	4.95	1.37E-08	1.68E-06	Itgb8	− 3.18	2.37E-06	1.67E-04
Efs	4.50	7.27E-04	1.73E-02	Ildr2	− 2.86	1.02E-03	2.27E-02
Arhgef15	3.74	4.95E-04	1.32E-02	Npy2r	− 2.77	1.34E-04	4.69E-03
Cyp4f14	3.36	3.36E-03	5.37E-02	Thsd4	− 2.77	1.82E-03	3.46E-02
Mesp2	3.36	3.36E-03	5.37E-02	Wnt16	− 2.66	3.26E-03	5.23E-02
Cyp1a1	3.13	2.12E-04	6.70E-03	1600002K03Rik	− 2.54	5.81E-03	7.68E-02
Ugt1a6a	2.95	7.17E-04	1.73E-02	Fzd9	− 2.54	5.81E-03	7.68E-02
Gm10639	2.85	1.31E-03	2.76E-02	Kap	− 2.49	1.99E-09	3.00E-07

involved in DN. These results showed that MIC-1 can partially reduce levels of negative impact on HG-treated MES13, which suggest that MIC-1 may have beneficial effect on HG-induced disorder in MES13.

Canonical Signaling Pathways Affected by HG and MIC-1 Treatment

Next, the potential canonical signaling pathways affected by HG and MIC-1 were interpreted by the IPA. Gene expression that showed |log2 fold change| ≥ 0.3 was used from the HG *vs.* LG group and HG plus MIC-1 *vs.* HG group. Based on the −log (*p* value) and activation *z* scores of the pathways generated by IPA, canonical signaling pathways were then selected. Interestingly, some of these pathways were activated by HG and inhibited by MIC-1, while some of them were inhibited by HG and activated by MIC-1. Among those pathways, 20 related pathways were selected from the IPA pathway analysis. As shown in Table III, pathways such as GNRH signaling, endocannabinoid neuronal synapse pathway, oxidative ethanol degradation III, calcium signaling, and thrombin signaling were inhibited by HG and activated by MIC-1 exposure. Pathways such as the P2Y purigenic receptor

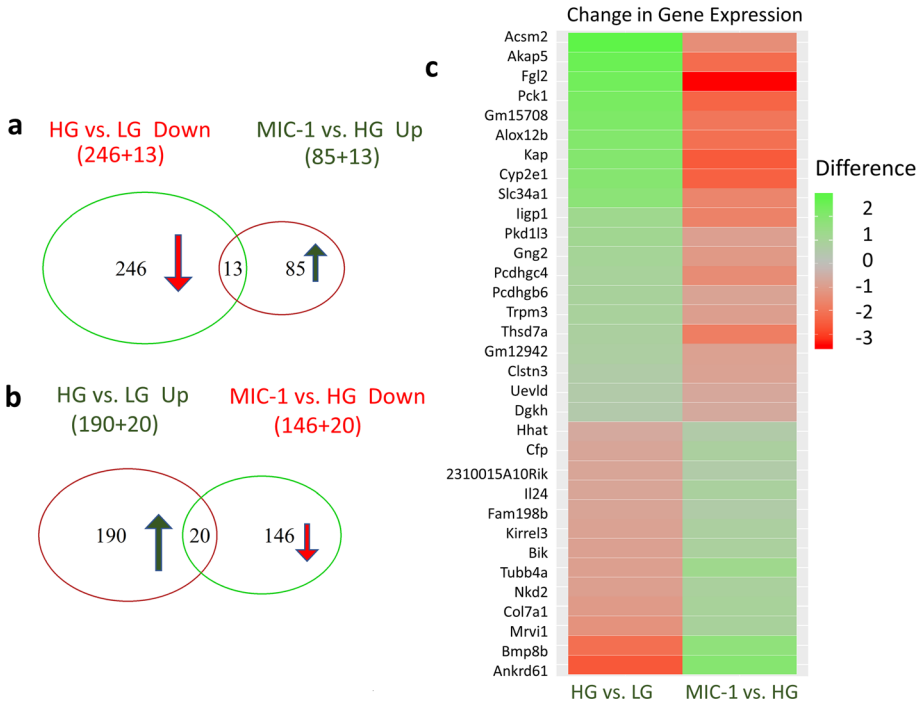

Fig. 4. Overview of differentially expressed genes between HG *vs.* LG and MIC-1 *vs.* HG. The Venn diagram showed 13 genes that were significantly downregulated by HG were upregulated after MIC-1 treatment (**a**), and 20 genes that were significantly upregulated by HG were downregulated after MIC-1 treatment (**b**). Heatmap of the 33 DEGs reversed by MIC-1 treatment (**c**). The color of the heatmap is equal to the log2 fold change in each comparison

Table III. 20 Altered Canonical Pathways Determined Using Ingenuity Pathway Software. Positive *z* Scores Suggest Pathway Activation and Negative *z* Scores Represent Pathway Inhibition

	HG *vs.* LG		MIC-1 *vs.* HG	
Ingenuity canonical pathways	−log (*p* value)	*z* score	−log (*p* value)	*z* score
GNRH signaling	3.81	− 0.26	4.93	0.60
Corticotropin-releasing hormone signaling	3.69	0.23	2.33	− 0.89
GPCR-mediated nutrient sensing in enteroendocrine cells	3.65	1.21	4.63	− 0.85
Dopamine-DARPP32 feedback in cAMP signaling	3.35	0.94	4.15	− 1.53
Endocannabinoid neuronal synapse pathway	2.97	− 1.21	3.73	0.85
P2Y purigenic receptor signaling pathway	2.84	1.07	4.73	− 1.71
Calcium signaling	2.74	− 2.32	2.84	1.34
Paxillin signaling	2.70	− 0.82	3.08	0.71
Thrombin signaling	2.62	− 1.81	3.92	1.40
Adrenomedullin signaling pathway	2.31	0.94	4.07	− 0.19
Agrin interactions at neuromuscular junction	2.31	− 0.82	1.91	0.63
LPS/IL-1-mediated inhibition of RXR function	2.28	1.41	2.59	− 1.16
Oxidative ethanol degradation III	2.23	− 0.45	1.77	1.34
Synaptic long-term depression	2.20	− 0.47	3.43	0.38
Endothelin-1 signaling	2.15	− 0.69	3.58	1.30
Aryl hydrocarbon receptor signaling	2.09	1.41	2.33	− 1.27
Pyrimidine deoxyribonucleotides de novo biosynthesis I	2.06	1.34	2.25	− 0.82
Ethanol degradation IV	1.90	− 0.45	1.46	1.34
Nitric oxide signaling in the cardiovascular system	1.48	− 0.91	1.06	0.58
Apelin cardiomyocyte signaling pathway	1.48	− 1.73	1.95	0.26

signaling pathway, LPS/IL-1-mediated inhibition of RXR function were activated by HG and inhibited by MIC-1 exposure.

Profiling of DNA Methylome of MES13 in Response to HG and MIC-1 treatment

Next, we performed DNA CpG Methyl-Seq on MES13 to observe whether HG treatment affected the profiling of DNA methylome and whether MIC-1 treatment reversed those changes. Figure 5a showed that DMRs were mainly located in the promoter and the distal intergenic region. Also, the distribution of DMRs indicated that, based on the number and region of CpGs, the number of CpG sites in the promoter region were greater than that in other regions such as gene body, 3′ UTRs, downstream, or 5′UTRs (Fig. 5b). Notably, the promoter region showed a lower average methylation level than other regions (Fig. 5c). To further analyze DNA methylation in the promoter region, DNA methylation profiles of LG treatment *vs.* HG or HG plus MIC-1 were compared. The overlapping genes showing reverse relationship between HG and MIC-1 treatment were identified using a cutoff threshold of 25% for DNA methylation ratio with p value < 0.01. As shown in Fig. 6, a total of 173 DMRs in the promoter region were detected between the HG group and LG group (71 DMRs were hypomethylated and 102 DMRs were hypermethylated related to HG). We also observed 149 DMRs between the HG with the MIC-1 group and the HG group (59 DMRs were hypermethylated and 90 DMRs were hypomethylated related to MIC-1). Interestingly, 4 DMRs in the promoter region were significantly hypomethylated by HG (4/71) but hypermethylated after MIC-1 treatment (4/59) (Fig. 6a). 16 DMRs in the promoter region were hypomethylated by HG (16/102) but hypermethylated after MIC-1 treatment (16/90) (Fig. 6b). These reversed DMRs by MIC-1 exposure were shown in the heatmap (Fig. 6c). Several of these genes including Vegfc (involved in endothelial cell function) and Cbx1 (involved in epigenetic control of chromatin structure and gene expression) are potentially involved in DN.

Correlation Between DNA Methylation and Transcription

Next, we analyzed the correlation between gene expression profile and promoter regions DNA methylation profile to understand the relationship between DNA methylation and gene expression. With a cutoff of methylation ratio difference (%) ≥ 10 for DNA methylation changes at the promoter regions and |log2 (fold change)| ≥ 1 changes for RNA expression, a total of 85 DEGs/DMRs were found in the HG *vs.* LG group (Supplementary Table 1). Of these 85 DEGs/DMRs in the promoter region, 38 DMRs showed inverse correlations with differential expression of the corresponding genes/RNA. As shown in Fig. 7a (Supplementary Table 1), each dot represents DEG/DMR in different promoter regions of the HG *vs.* LG group. Similarly, a total of 267 DEGs/DMRs were found in the MIC-1 group *vs.* HG group (Fig. 7b; Supplementary Table 2). Of these 267 DEGs/DMRs in the promoter region, 140 DMRs showed inverse correlations with differential expression of the corresponding genes/RNA. As shown in Fig. 7b, each dot represents DEG/DMR and their corresponding gene features are indicated by different colors in the MIC-1 group *vs.* HG group. Integrative analysis of RNA-Seq and DNA-Seq data yields a subset of genes associated with HG and MIC-1 treatment, and the gene expression changes may be driven by promoter CpG status; these genes include Col4a2 (involved in basement membrane remodeling), Tceal3 (involved in transcriptional control), Apoe (involved in lipid metabolism),

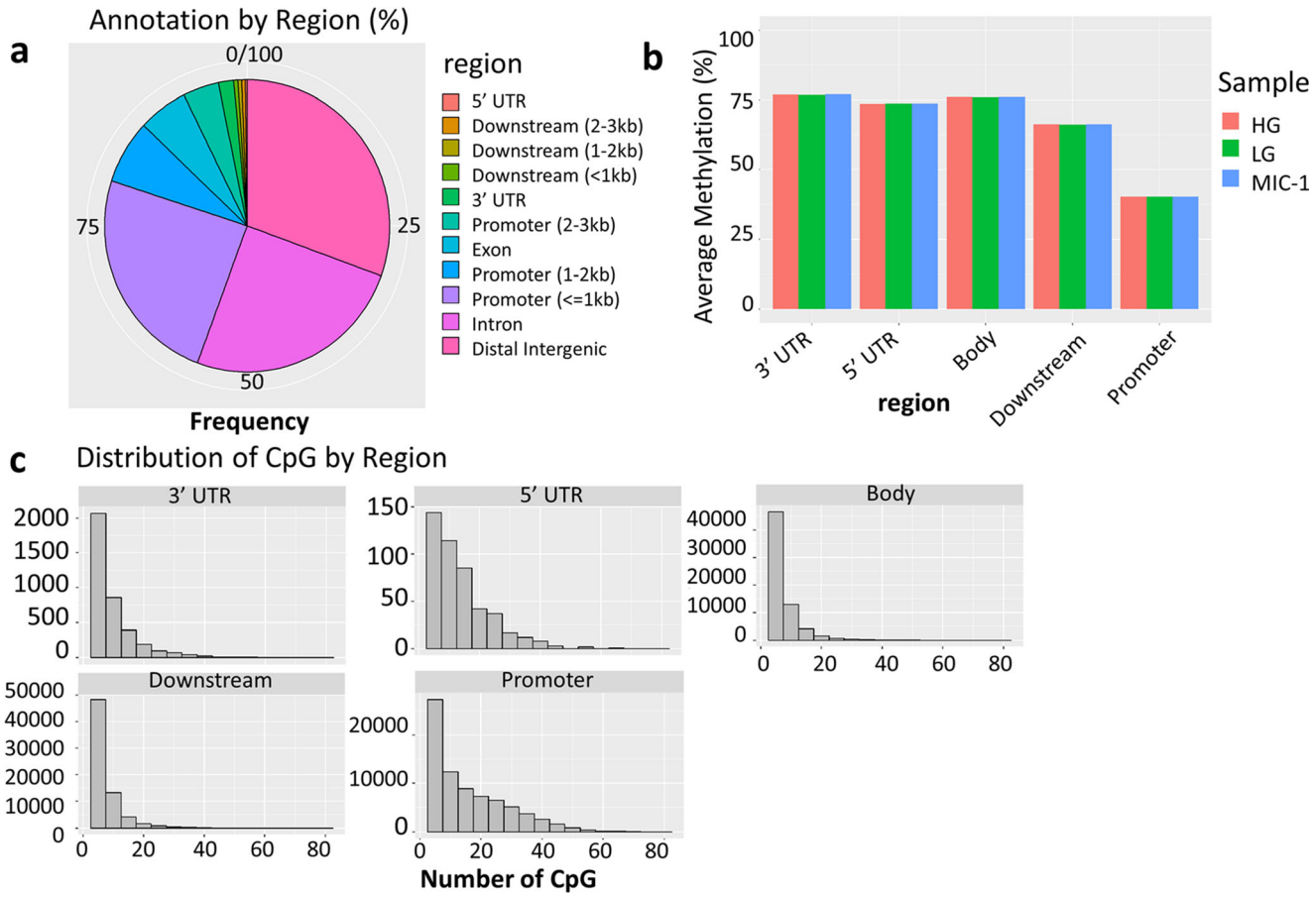

Fig. 5. Overview of the DNA methylation profile. **a** Frequency of annotated DMRs by feature. **b** Distribution of DMRs by the number of CpGs and region. **c** Average methylation levels of DMRs based on gene regions in all the 3 groups

Esam (involved in endothelial cell function), and Agt (involved in the angiotensin pathway).

DISCUSSION

Accumulating evidence has shown that excessive oxidative stress and inflammation are responsible for the development of DN (32,33). HG environment can stimulate excessive ROS production which can contribute to DN (34,35). Previously, it was reported that MIC-1 possesses anti-inflammatory and antioxidant properties (17,36). However, the epigenome and transcriptome effects of MIC-1 in MES13 challenged with HG, a pre-condition for diabetic nephropathy remain unknown. In our current study, we investigated the alteration of basal DNA methylation and gene expression when MES13 were subjected to HG, and the impact of MIC-1 treatment on these changes. Our results showed that HG can change some gene expression and DNA methylation level in the MES13, and MIC-1 can reverse some epigenomic and transcriptomic changes.

It is well known that Nrf2 related to cytoprotection and its reactivation in oxidative stress injury result due to ROS or electrophiles (33,37). More and more evidence indicated that the Nrf2 pathway and DN have cross talk in different stages. We have previously shown that MIC-1 activates Nrf2 signaling, increases expression of Nrf2-mediated gene NAD(P)H/quinone oxidoreductase 1 (NQO1), heme oxygenase-1 (HO-1), and suppresses inflammation, thereby also reducing oxidative stress in HG-induced human renal proximal tubule HK-2 cells (17). In our study, we found that some of these pathways were activated by HG and inhibited by MIC-1, while some of them were inhibited by HG and activated by MIC-1. Pathways such as GNRH signaling, endocannabinoid neuronal synapse pathway, oxidative ethanol degradation III, calcium signaling, and thrombin signaling were inhibited by HG and activated by MIC-1 exposure. Pathways such as the P2Y purigenic receptor signaling pathway and LPS/IL-1-mediated inhibition of RXR function were activated by HG and inhibited by MIC-1 exposure. Previous studies have found that Nrf2 regulates antioxidant response element to activate target genes and thus participate in the anti-oxidative stress/anti-inflammatory process (38,39). Moreover, previous evidence showed that oral administration of MIC-1-enriched Moringa seed extract ameliorated ulcerative colitis symptoms and associated biomarkers in both dextran sulfate sodium (DSS)-induced acute and chronic ulcerative colitis mouse models by regulating inflammatory and antioxidant properties (36). These results suggest that MIC-1 may potentially activate NRF2-mediated oxidative stress pathway and suppress inflammatory responses induced by HG.

CpG methylation is a reversible epigenetic modification that can regulate gene expression in response to intrinsic and extrinsic stimuli (40). Aberrant epigenetic states have been observed in the progression of DN (9,41). In our current study, we found that the average methylation of promoter regions was

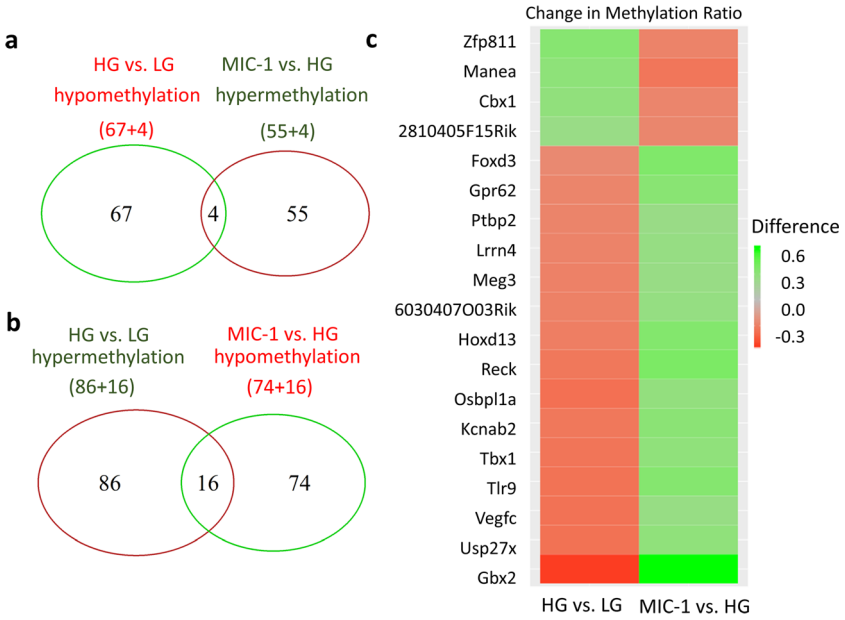

Fig. 6. Promoter methylation changes following MIC-1 exposure. The Venn diagram showed 4 DMRs in the promoter region were significantly hypomethylated by HG but hypermethylated by MIC-1 treatment (**a**), and 16 DMRs in the promoter region were hypomethylated by HG but hypermethylated by MIC-1 treatment (**b**) using a cutoff threshold methylation difference greater than 25% with p value 0.01. Heatmap of the overlapping DMRs between the two comparisons (**c**). The color of the heatmap is equal to the methylation difference in each comparison

lower than that of other regions including 3′UTR, 5′UTR, gene body, and downstream. We identified HG- or MIC-1-associated changes in the methylation status of the promoter in MES13. It has been shown that promoter methylation is a characteristic of suppressed transcription of the genes, and gene body methylation is frequently associated with active transcription of genes (42). Therefore, we analyzed the potential correlation between DNA methylation status and gene expression. As shown in Fig. 7, both DNA methylation in the promoter regions and the corresponding transcription change were identified. These results agree with the previous study, showing DNA demethylation correlates with gene expression and could be an important therapeutic target in cancer and carcinogenesis (43). Our current data showed that after HG and MIC-1 exposure, gene expression was downregulated along with hypermethylation in some promoter regions. It can be speculated that the genes may

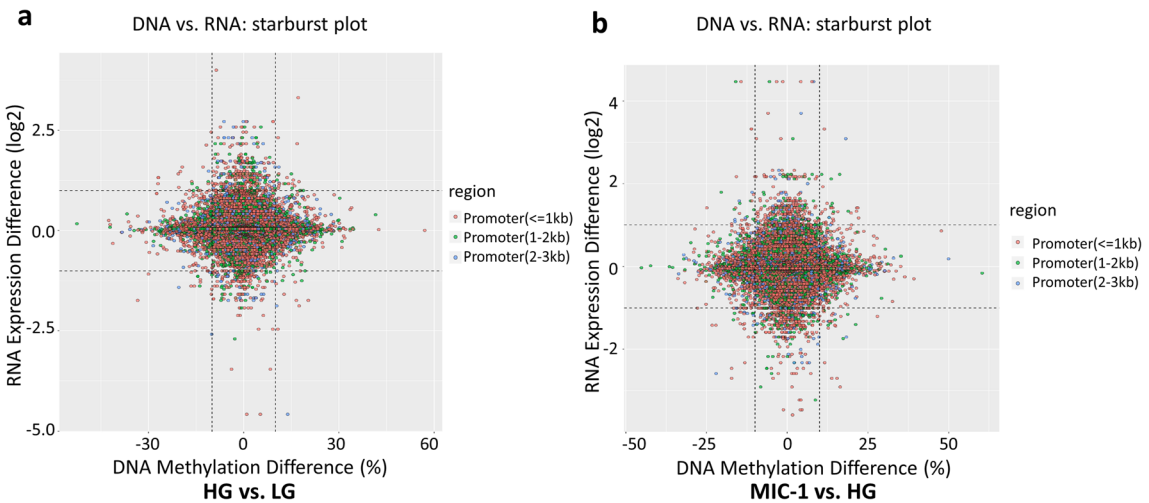

Fig. 7. Correlations between gene expression and promoter DNA methylation by a cutoff methylation ratio difference (%) ≥ 10 for promoter DNA methylation change and a |log2 (fold change)| ≥ 1 change threshold for RNA expression. **a** Scatter plot showing DMRs/genes in the HG *vs.* LG group. **b** Scatter plot showing DMRs/genes in the MIC-1 *vs.* HG group. The DMR locations (gene features) are indicated by different colors

be regulated by promoter methylation in response to MIC-1 treatment.

CONCLUSION

To sum up, this research investigated the effects of MIC-1 in the HG-induced DN cell model in the mouse kidney mesangial cells by the latest RNA-Seq and Methyl-Seq technology. Integrative analysis of omics data yielded a subset of genes associated with MIC-1 treatment, and the gene expression changes may be driven by promoter CpG status. Canonical pathways showed that MIC-1 could partially attenuate the levels of negative impact of HG-treated MES13. Our current study provides novel insights into the epigenomic and transcriptomic alterations when MES13 were challenged by HG, a pre-condition of DN, and most importantly, MIC-1 treatment can reverse some of the pathways/genes impacted by HG, which may help to identify potential therapeutic targets and strategies for DN.

FUNDING INFORMATION

This study was supported by R01AT009152 from the National Center for Complementary & Alternative Medicine (NCCAM) and R01CA200129 from the National Cancer Institute (NCI). The authors appreciate all the members of Dr. Kong's laboratory for their invaluable support and technical assistance.

COMPLIANCE WITH ETHICAL STANDARDS

Conflict of Interest The authors declare that they have no conflict of interest.

REFERENCES

1. Thomas MC, Cooper ME, Zimmet P. Changing epidemiology of type 2 diabetes mellitus and associated chronic kidney disease. Nat Rev Nephrol. 2016;12(2):73–81.
2. Tuttle KR, Bakris GL, Bilous RW, Chiang JL, De Boer IH, Goldstein-Fuchs J, et al. Diabetic kidney disease: a report from an ADA Consensus Conference. Am J Kidney Dis. 2014;64(4):510–33.
3. de Boer IH, Rue TC, Hall YN, Heagerty PJ, Weiss NS, Himmelfarb J. Temporal trends in the prevalence of diabetic kidney disease in the United States. Jama. 2011;305(24):2532–9.
4. Shahbazian H, Rezaii I. Diabetic kidney disease; review of the current knowledge. J Renal Injury Prevent. 2013;2(2):73–80.
5. Yaribeygi H, Atkin SL. Interleukin-18 and diabetic nephropathy: a review. 2019;234(5):5674–82.
6. Lim AK, Tesch GH. Inflammation in diabetic nephropathy. Mediators of Inflammation 2012;2012:146154.
7. Medzhitov R. Origin and physiological roles of inflammation. Nature. 2008;454(7203):428–35.
8. Kashihara N, Haruna Y, Kondeti KV, Kanwar SY. Oxidative stress in diabetic nephropathy. Curr Med Chem. 2010;17(34):4256–69.
9. Kato M, Natarajan R. Diabetic nephropathy—emerging epigenetic mechanisms. Nat Rev Nephrol. 2014;10(9):517–30.
10. Lu Z, Liu N, Wang F. Epigenetic regulations in diabetic nephropathy. J Diabetes Res. 2017;2017:7805058.
11. Huang D, Cui L, Ahmed S, Zainab F, Wu Q, Wang X, et al. An overview of epigenetic agents and natural nutrition products targeting DNA methyltransferase, histone deacetylases and microRNAs. Food Chem Toxicol. 2019;123:574–94.
12. Guo Y, Su Z-Y, Kong A-NT. Current perspectives on epigenetic modifications by dietary chemopreventive and herbal phytochemicals. Curr Pharmacol Rep. 2015;1(4):245–57.
13. Yuqing Yang A, Kim H, Li W, Tony Kong A-N. Natural compound-derived epigenetic regulators targeting epigenetic readers, writers and erasers. Curr Top Med Chem. 2016;16(7):697–713.
14. Bennett RN, Mellon FA, Foidl N, Pratt JH, Dupont MS, Perkins L, et al. Profiling glucosinolates and phenolics in vegetative and reproductive tissues of the multi-purpose trees Moringa oleifera L. (Horseradish tree) and Moringa stenopetala L. J Agric Food Chem. 2003;51(12):3546–53.
15. Leone A, Spada A, Battezzati A, Schiraldi A, Aristil J, Bertoli S. Cultivation, genetic, ethnopharmacology, phytochemistry and pharmacology of Moringa oleifera leaves: an overview. Int J Mol Sci. 2015;16(6):12791–835.
16. Yassa HD, Tohamy AF. Extract of Moringa oleifera leaves ameliorates streptozotocin-induced diabetes mellitus in adult rats. Acta Histochem. 2014;116(5):844–54.
17. Cheng D, Gao L, Su S, Sargsyan D, Wu R, Raskin I, et al. Moringa isothiocyanate activates Nrf2: potential role in diabetic nephropathy. AAPS J. 2019;21(2):31.
18. Wang C, Wu R, Sargsyan D, Zheng M, Li S, Yin R, et al. CpG methyl-seq and RNA-seq epigenomic and transcriptomic studies on the preventive effects of Moringa isothiocyanate in mouse epidermal JB6 cells induced by the tumor promoter TPA. J Nutr Biochem. 2019;68:69–78.
19. Kim D, Li HY, Lee JH, Oh YS, Jun H-S. Lysophosphatidic acid increases mesangial cell proliferation in models of diabetic nephropathy via Rac1/MAPK/KLF5 signaling. Exp Mol Med. 2019;51(2):18.
20. Yano N, Suzuki D, Endoh M, Zhao TC, Padbury JF, Tseng Y-T. A novel phosphoinositide 3-kinase-dependent pathway for angiotensin II/AT-1 receptor-mediated induction of collagen synthesis in MES-13 mesangial cells. J Biol Chem. 2007;282(26):18819–30.
21. Yano N, Suzuki D, Endoh M, Cao TN, Dahdah JR, Tseng A, et al. High ambient glucose induces angiotensin-independent AT-1 receptor activation, leading to increases in proliferation and extracellular matrix accumulation in MES-13 mesangial cells. Biochem J. 2009;423(1):129–43.
22. Ho C, Lee PH, Hsu YC, Wang FS, Huang YT, Lin CL. Sustained Wnt/beta-catenin signaling rescues high glucose induction of transforming growth factor-beta1-mediated renal fibrosis. Am J Med Sci. 2012;344(5):374–82.
23. Catherwood MA, Powell LA, Anderson P, McMaster D, Sharpe PC, Trimble ER. Glucose-induced oxidative stress in mesangial cells. Kidney Int. 2002;61(2):599–608.
24. Shendure J, Ji H. Next-generation DNA sequencing. Nat Biotechnol. 2008;26(10):1135–45.
25. Goodwin S, McPherson JD, McCombie WR. Coming of age: ten years of next-generation sequencing technologies. Nat Rev Genet. 2016;17(6):333–51.
26. Zhang Z, Yuan W, Sun L, Szeto F, Wong K, Li X, et al. 1,25-Dihydroxyvitamin D3 targeting of NF-κB suppresses high glucose-induced MCP-1 expression in mesangial cells. Kidney Int. 2007;72(2):193–201.
27. Li W, Sargsyan D, Wu R, Li S, Wang L, Cheng D, et al. DNA methylome and transcriptome alterations in high glucose-induced diabetic nephropathy cellular model and identification of novel targets for treatment by tanshinone IIA. Chem Res Toxicol. 2019;32:1977–88.
28. Yang Y, Wu R, Sargsyan D, Yin R, Kuo H-C, Yang I, et al. UVB drives different stages of epigenome alterations during progression of skin cancer. Cancer Lett. 2019;449:20–30.
29. Guo Y, Wu R, Gaspar JM, Sargsyan D, Su Z-Y, Zhang C, et al. DNA methylome and transcriptome alterations and cancer prevention by curcumin in colitis-accelerated colon cancer in mice. Carcinogenesis. 2018;39(5):669–80.
30. Storey JD. The positive false discovery rate: a Bayesian interpretation and the q-value. Ann Stat. 2003;31(6):2013–35.

31. Gaspar JM, Hart RP. DMRfinder: efficiently identifying differentially methylated regions from MethylC-seq data. BMC Bioinf. 2017;18(1):528.
32. Elmarakby AA, Sullivan JC. Relationship between oxidative stress and inflammatory cytokines in diabetic nephropathy. Cardiovasc Ther. 2012;30(1):49–59.
33. Ruiz S, Pergola PE, Zager RA, Vaziri ND. Targeting the transcription factor Nrf2 to ameliorate oxidative stress and inflammation in chronic kidney disease. Kidney Int. 2013;83(6):1029–41.
34. Ha H, Lee HB. Reactive oxygen species as glucose signaling molecules in mesangial cells cultured under high glucose. Kidney Int. 2000;58:S19–25.
35. Inoguchi T, Li P, Umeda F, Yu HY, Kakimoto M, Imamura M, et al. High glucose level and free fatty acid stimulate reactive oxygen species production through protein kinase C–dependent activation of NAD (P) H oxidase in cultured vascular cells. Diabetes. 2000;49(11):1939–45.
36. Kim Y, Wu AG, Jaja-Chimedza A, Graf BL, Waterman C, Verzi MP, et al. Isothiocyanate-enriched moringa seed extract alleviates ulcerative colitis symptoms in mice. PLoS One. 2017;12(9):e0184709.
37. Uruno A, Motohashi H. The Keap1–Nrf2 system as an in vivo sensor for electrophiles. Nitric Oxide. 2011;25(2):153–60.
38. Ahmed SMU, Luo L, Namani A, Wang XJ, Tang X. Nrf2 signaling pathway: pivotal roles in inflammation. Biochim Biophys Acta (BBA)-Mol Basisf Dis. 2017;1863(2):585–97.
39. Itoh K, Mochizuki M, Ishii Y, Ishii T, Shibata T, Kawamoto Y, et al. Transcription factor Nrf2 regulates inflammation by mediating the effect of 15-deoxy-Δ12, 14-prostaglandin J2. Mol Cell Biol. 2004;24(1):36–45.
40. Esteller M. Epigenetics in cancer. N Engl J Med. 2008;358(11):1148–59.
41. Oba S, Ayuzawa N, Nishimoto M, Kawarazaki W, Ueda K, Hirohama D, et al. Aberrant DNA methylation of Tgfb1 in diabetic kidney mesangial cells. Sci Rep. 2018;8(1):16338.
42. Jones PA. Functions of DNA methylation: islands, start sites, gene bodies and beyond. Nat Rev Genet. 2012;13(7):484–92.
43. Yang X, Han H, De Carvalho DD, Lay FD, Jones PA, Liang G. Gene body methylation can alter gene expression and is a therapeutic target in cancer. Cancer Cell. 2014;26(4):577–90.